International Journal of Aeronautical and Space Sciences (2019) 20:850–857
https://doi.org/10.1007/s42405-019-00175-4

IJASS International Journal of Aeronautical and Space Sciences

ORIGINAL PAPER

Effect of Inlet Boundary Layer Suction on Flow Distortion in Subsonic Diffusing S-Duct

Jihyeong Lee[1] · Seawook Lee[2] · Jinsoo Cho[3]

Received: 16 October 2018 / Revised: 19 February 2019 / Accepted: 20 February 2019 / Published online: 24 May 2019

Abstract
The effects of the boundary layer suction (BLS) near the S-duct inlet on the flow distortion of the S-duct were analyzed using a commercial computational fluid dynamics tool. The purpose of this study was to investigate the effect of shape factors on the location and length of the BLS for the RAE M 2129 S-duct with the inlet shape AR (0.75,0). The performance of the S-duct is influenced by the boundary layer thickness for duct flow and the counter-rotating vortex position on the engine face. All of the cases upon applying BLS were confirmed as having a different boundary layer thickness and the counter-rotating vortex at the engine face was confirmed. The PS (0,0.1) case has the thinnest boundary layer and the counter-rotating vortex is the farthest from the starboard side, while the PS (0.06,0.08) case has the thickest boundary layer and the counter-rotating vortex is located near the starboard side. In conclusion, it was confirmed that BLS has a significant influence on the flow distortion for the applied position compared to the applied length. Additionally, the PS (0,0.1) case applied near duct inlet showed the least flow distortion, and the PS (0.06,0.08) case located near the cowl lip showed the largest flow distortion.

Keywords Boundary layer suction · Counter-rotating vortex · Boundary layer thickness · Flow distortion

1 Introduction

Generally, aircraft propulsion systems are divided into podded and embedded types. An embedded propulsion system is a propulsion system in which the engine is located inside the fuselage, and an intake is necessary to supply air to the engine [1]. The intake is a duct required to ensure smooth air flow to the engine, while minimizing pressure loss and flow distortion, thereby delivering the pressure distribution uniformly to the engine [2]. An intake that is short with a straight-line shape has less flow loss, but military aircraft such as a fighter aircraft typically have an S-shaped duct with curvature to achieve a more compact aircraft system, lower observability, and reduced drag. At this time, an S-shaped duct with a curvature is defined as an S-duct [3]. An S-duct causes flow separation and secondary flow due to the inlet shape, including the offset between the duct inlet and the engine face, the curvature, the area ratio, and the intake flow at the inlet [4]. Specifically, the intake flow at the duct inlet determines performance depending on the state of the developed flow at the duct surface and the shape of the S-duct [5, 6]. Wagner et al. [7, 8] studied the effect of the inlet boundary layer on the flow field inside the compressor and confirmed that the hub corner stall and tip leakage flow have different characteristics depending on the inlet boundary layer thickness. Ki [9] studied the influence of the boundary layer diverter on the performance of the air intake port, which separates the boundary layer flow developed from the fuselage from the inlet flow, and then determined the height of the minimum boundary layer diverter to maintain the air inlet performance. In addition, many previous studies have analyzed the internal duct flow characteristics by applying flow control to a supersonic intake, and then investigated methods to improve the duct performance. Debiasi et al. [10] conducted a study to improve the

✉ Jinsoo Cho
jscho@hanyang.ac.kr

Jihyeong Lee
ghok0070@gmail.com

Seawook Lee
swlee@shtouch.co.kr

[1] Department of Mechanical Engineering, Hanyang University, Seoul, Republic of Korea

[2] R&D Center, IBIRDIE, Seoul, Republic of Korea

[3] School of Mechanical Engineering, Hanyang University, Seoul, Republic of Korea

performance of flow distortion and total pressure recovery by injecting a constant amount of flow to the S-duct inlet and applying suction at the same amount of flow near the engine face. As a result, the reduction of the separation bubble and reattachment due to inhalation were confirmed. Scribben et al. [11] measured total pressure by injecting 1% of the inlet mass flow rate into a curved duct. The flow distortion was improved by approximately 70% in the duct inlet region and the total pressure recovery rate was improved by about 2%. Choi et al. [12] have investigated the effect of the position and number of bleeding flow controls on the duct performance with respect to the ram jet inlet. Gary et al. [13] proposed the existing boundary layer bleed removal design and presented a new model utilizing a bleed hole and narrow slot. Slater [14] proposed an improved bleed model using scaling of sonic coefficient data for 90° bleeding holes. Willis et al. [15, 16] investigated a boundary layer control via mass flow removal. The *l*/*d* ratio was confirmed to influence the flow characteristics of the bleed orifice. Liou et al. [17] optimized the bleed at the supersonic inlet. Optimization was performed with the position and flow rate of the bleed as variables, and proposed the importance of low-energy flow control before flow separation.

To improve the performance of the S-duct applied to the fuselage, an active flow control method using boundary layer suction and a passive flow control method using the boundary layer diverter were applied to perform a study. However, knowledge of the relationship between mass flow, position, angle, shape, and aerodynamic performance on the influence of the boundary layer suction and flow in an S-duct is insufficient.

In this study, the effects of the boundary layer suction on the internal flow of the subsonic S-duct applied to the flat plate were studied. Boundary layer suction was applied near the duct inlet, and this study used the location and area of the boundary layer suction as variables for the same mass flow.

2 Computational Method

2.1 Geometry of the S-Duct

The model investigated in this study is the RAE M 2129 S-duct having an upper semi-circular inlet shape with an upper half aspect ratio (AR_{upper}) of 0.75 and a lower half aspect ratio (AR_{lower}) of 0 (AR 0.75,0), which was proposed by Lee et al. [18]. The definition of the inlet shape is shown in Fig. 1 and Eqs. (1)–(3). The RAE M 2129 S-duct was used to study flow characteristics and main factor effects on S-duct performance [19]. The S-duct has a diffuser shape that has an increasing area along the centerline. The centerline is defined as the line passing through the inward center of the semicircular inner (core) and the inner center of the engine face as shown in Eq.

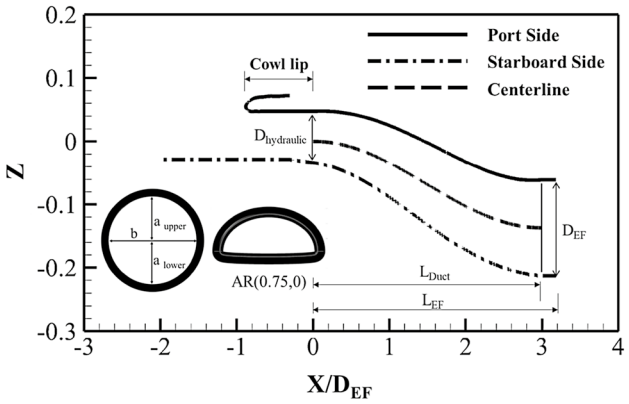

Fig. 1 RAE M 2129 S-duct with inlet shape AR (0.75,0) geometry

Table 1 S-duct with inlet shape AR (0.75,0) shape parameter

Parameter	Value (m)	Description
$D_{hydraulic}$	0.0992	Hydraulic diameter
D_{EF}	0.1524	Engine face diameter
CR	0.9177	Contraction ratio
L_{EF}	0.4839	S-duct length
L_{Duct}	0.4572	Engine face location

(4), the definition of cross-sectional area along the curvature line is given by Eq. (5). The geometry of the S-duct is defined as a few shape parameters, as shown in Fig. 1, which appear on the port and starboard sides within the *x*–*z* plane. The parameter values for the S-duct are given in Table 1:

$$a_{upper} = AR_{upper}\sqrt{\frac{2\times A}{(AR_{upper}+AR_{lower})\pi}}, \tag{1}$$

$$a_{lower} = AR_{lower}\sqrt{\frac{2\times A}{(AR_{upper}+AR_{lower})\pi}}, \tag{2}$$

$$b = \sqrt{\frac{2\times A}{(AR_{upper}+AR_{lower})\pi}}, \tag{3}$$

where A is the area, AR_{upper} is the upper half aspect ratio, AR_{lower} is the lower half aspect ratio, a_{upper} is the upper vertical length, a_{lower} is the lower vertical length, and b is the horizontal length;

$$C = -0.15L_{Duct}\left[1-\cos\left(\frac{\pi X}{L_{Duct}}\right)\right], \tag{4}$$

$$\left(\frac{A-A_{\text{throat}}}{A_{\text{engine face}}-A_{\text{throat}}}\right) = \left(3\left(1-\frac{X}{L_{\text{Duct}}}\right)^4 - 4\left(1-\frac{X}{L_{\text{Duct}}}\right)^3 + 1\right). \quad (5)$$

2.2 Definition of the Boundary Layer Suction

To investigate the influence of the boundary layer suction near the inlet of the S-duct as applied to the flat plate on the internal flow characteristics, boundary layer suction design factors were defined. The design factors were the BLS location and length with mass flow fixed area. The location of BLS was defined by distance in the negative x-direction, and the width of BLS was fixed to the horizontal length of the inlet of AR (0.75,0) model, and the influence of BLS on the velocity distribution was studied with length as a variable. The mass flow rate was set at 1% with respect to the mass flow rate at the engine face of the model without BLS which is RAE M 2129 S-duct having an upper semi-circular with AR (0.75,0) inlet shape. The range of the design factors was defined to the extent that the effect of the BLS is until insignificant. The model work performed according to the BLS shape included 40 models with eight location cases (0–0.14, interval 0.02, unit: m) and five area cases (0.02–0.1, interval 0.02, unit: m). The definition of boundary layer suction is shown in Fig. 2.

2.3 Performance Factors

To investigate the aerodynamic characteristics of the S-duct with boundary layer suction, the main performance factors were used. The main performance factors of the S-duct were pressure recovery and distortion coefficient as represented by Eqs. (6–8) [20]. Pressure recovery represents the average level of total pressure conservation at the engine face when freestream reaches the engine through the duct inlet. The smaller the pressure recovery (closer to 0) value, the more likely thrust loss will occur, while greater pressure recovery (closer to 1) values indicate better S-duct performance. The distortion coefficient represents the degree of flow uniformity at the engine face. In contrast to the pressure recovery value, the distortion coefficient is uniform flow as the distortion coefficient is closer to 0, and the flow distortion is non-uniform flow as closer to 1. There is a risk of engine surge when the flow distortion is severe. P_{TEF60} of the distortion coefficient is the total pressure in the 60° fan-shaped region of the engine face. As shown in Fig. 3, the 60° fan-shaped region was the lowest value of the total pressure next to the ϕ region [21]. The uniform flow index is a performance factor for evaluating the flow uniformity in the duct cross section. The perfect flow uniformity approaches a value of 1, while non-uniformity is closer to 0 [22, 23]:

$$\text{Pressure recovery}: \text{PR} = \frac{P_{\text{T}_{\text{EF}}}}{P_{\text{T}_{\text{avi}}}}, \quad (6)$$

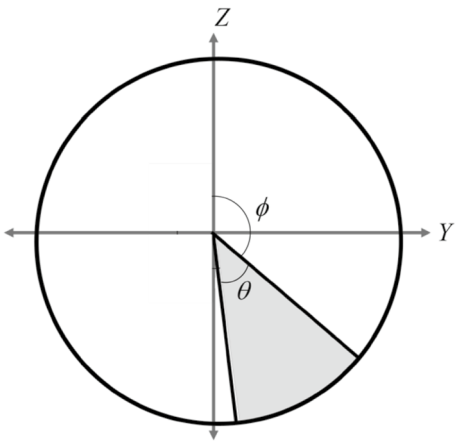

Fig. 3 Definition of the engine face distortion

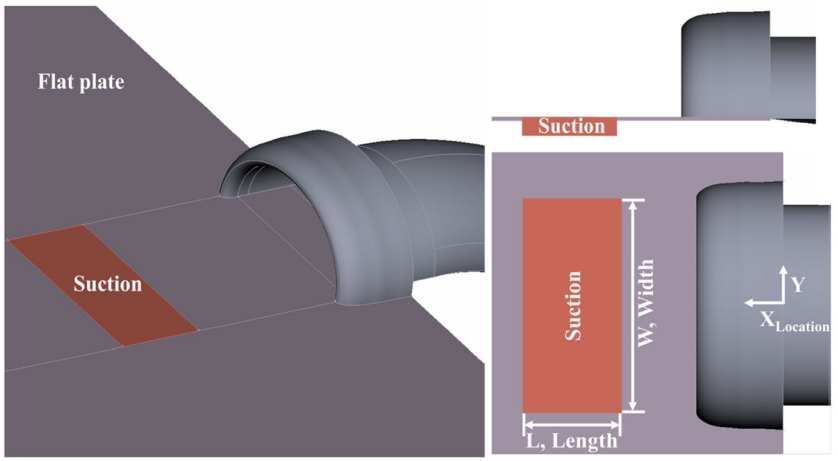

Parameter	Location	Length
Upper Bound [m]	0	0.02
Lower Bound [m]	0.14	0.1
Step [m]	0.02	0.02

Fig. 2 Definition of boundary layer suction

where $P_{T_{EF}}$ is the total pressure at engine face, and $P_{T_{avi}}$ is the total pressure at inlet;

$$\text{Distortion coefficient}: \text{DC60} = \frac{\max\left[\left|P_{T_{EF}} - P_{T_{EF60}}\right|\right]}{0.5\rho u_{ave}^2}, \tag{7}$$

where $P_{T_{EF}}$ is the total pressure at engine face, $P_{T_{EF60}}$ is the total pressure at worst 60° sector of engine face, ρ is the density at engine face, and u_{ave} is the mass average velocity at engine face;

$$\text{Uniform flow index}: \gamma = 1 - \frac{\sum_{i=1}^{n} \frac{\sqrt{(u_i - \bar{u})^2}}{\bar{u}} \cdot A_i}{2 \cdot A_{cell_{tot}}}, \quad \bar{u} = \frac{\sum_{i=1}^{n} u_i \cdot A_i}{A_{cell_{tot}}}, \tag{8}$$

where γ is the uniformity index, A_i is the local cell area, $A_{cell_{tot}}$ is the total cell area, n is the number of cells, u_i is the local velocity, and $\bar{u}$ is the mean velocity.

2.4 Governing Equation and Turbulence Model

The aerodynamic characteristics of the S-duct with boundary layer suction were investigated using the commercial solver ANSYS-CFX Ver. 17.2, which employs the three-dimensional Reynolds averaged Navier–Stokes (RANS) equations using a pressure-based coupled solver and a finite volume method. The RANS equations are composed of continuity, momentum, and energy equations, as given by Eqs. (6–8) [24]. Discretization of the governing equation was used to generate a high-resolution scheme in the form of a second-order method. The turbulence model used the k–ω SST model, which combines the advantages of k–ω to perform relatively accurate predictions in the boundary layer region and the advantage of k–ε to accurately predict the boundary layer outer region. The present turbulence model has advantages in predicting the adverse pressure gradient by viscosity, as well as advantages for the flow separation and secondary flow prediction [25]:

$$\text{Continuity equation:} \frac{\partial \rho}{\partial t} + \nabla \bullet (\rho U) = 0, \tag{9}$$

$$\text{Momentum equation:} \frac{\partial(\rho U)}{\partial t} + \nabla \bullet (\rho U \times U) = -\nabla p + \nabla \bullet \tau + S_M, \tag{10}$$

$$\text{Energy equation:} \frac{\partial\left(\rho h_{tot}\right)}{\partial t} - \frac{\partial p}{\partial t} + \nabla \bullet \left(\rho U h_{tot}\right) = \nabla \bullet (\lambda \nabla T) + \nabla \bullet (U \cdot \tau) + U \bullet S_M + S_E\,. \tag{11}$$

2.5 Computational Domain and Boundary Conditions

The computational region was composed of a single flow field including external flow and internal flow. The radius of the external flow field is 18 times larger than the radius of the engine face. Because there were no influences of the S-duct cowl lip or flat plate [4].

The Reynolds number was 777,000 based on the engine face diameter for the experimental boundary condition defined by the Aircraft Research Association (ARA) [26]. Boundary conditions on the external flow region were applied for Riemann invariant conditions. A no-slip condition was set for the wall surface and flat plate of the duct. The boundary condition of the engine face was set for the back pressure condition and it was set based on the engine inlet boundary condition proposed by Menzies [4]. Detailed boundary conditions are shown in Table 2, which were the applied conditions of the AGARD [27]: low mass flow rate of "Test Case3.2 (DP3537)" (LMFR). In Table 2, the incidence angle and angle of attack are defined as the angle in the x–z plane and the angle in the x–y plane, respectively.

The boundary condition for the BLS was set to the direction in which the mass flow was sucked, and a value of 1% was given to the mass flow rate at the engine face on the base model. Additionally, the boundary conditions were set by referring to the previous study [10–12], and the mass flow rate was set assuming that porosity value was 1. Figure 4 shows a computational grid. These grid units were composed of tetrahedral and prisms, which has a $y^+ = 1$ to predict secondary flow due to the adverse pressure gradient at the wall of the S-duct and flat plate.

2.6 Grid Independency Test

Since the analytical results show sensitive differences according to the size and number of grids generated in the computational analysis region, it is necessary to minimize the error of the result according to the number of grids. Therefore, the independence of the grid on the S-duct applied to the flat plate model used in this study has been

Table 2 Boundary conditions

	Value	Unit
Total pressure, $P_{T_{avi}}$	0.101134	MPa
Total temperature, T_{avi}	293	K
Flight Mach number, M_0	0.21	
Capture ratio	1.5428	
Angle of attack	0	°
Incidence angle	0	°

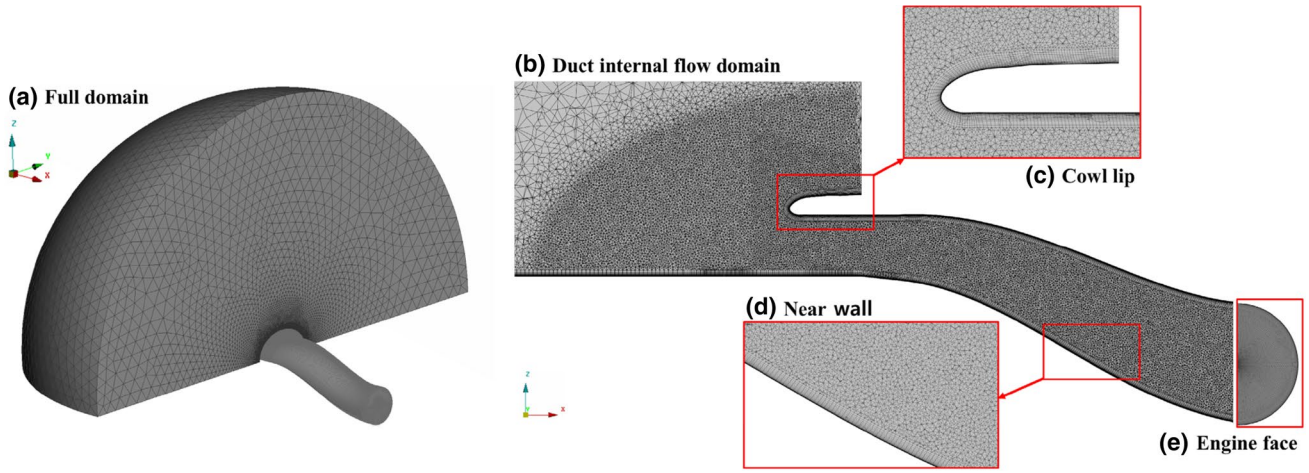

Fig. 4 Computational grid

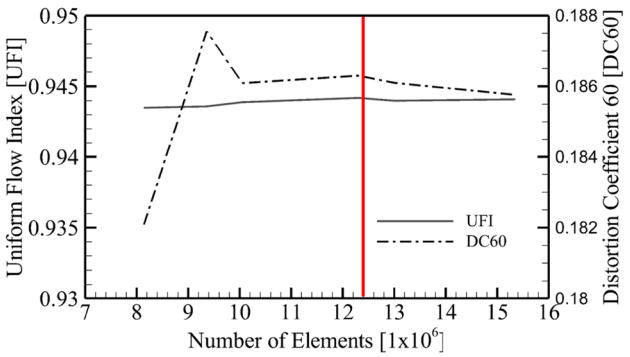

Fig. 5 Grid independence test

verified. The distortion coefficient values were compared by varying the number of gratings in the same flow region from 8 to 15 million as shown in Fig. 5. As a result, the error rate was less than 0.3% in the case of 12 million or more grids. Therefore, the number of grids utilized was approximately 12 million for performing the study, and the same number of grids was regenerated in the case of boundary layer suction.

3 Results

3.1 Aerodynamic Characteristics of S-Duct with Flat Plate

Figure 6 shows the flow characteristics in terms of the Mach number of the longitudinal plane and the uniform flow index of the cross-sectional area along the flow direction for the basic shape without BLS applied. As shown by the Mach number contour, the flow inside the duct moves from the starboard side to the port side due to the energy loss caused by the curvature of the duct. From $X/D_{EF} = 1.5$ with the greatest curvature, it was confirmed that the flow separation and the secondary flow were generated by the adverse pressure gradient. Also, as shown in the uniform flow contour for each section, the closer the flow is to the engine face, the more the counter-rotating vortex develops on the starboard side and the lower the uniform flow index value. It is thought that the flow becomes more non-uniform as the flow moves to the engine face.

3.2 Distortion Coefficient

Figure 7 is a bar graph comparing the DC60 values for all cases where BLS is applied. This graph shows the effects on the position and length of BLS. It can be seen that there is no large difference in the flow distortion with respect to the length variation of BLS, but it is confirmed that the degree of flow distortion varies greatly depending on the BLS position. In particular, it was confirmed that the effect of BLS applied in the region from the beginning of duct to before the cowl lip is large, and that the BLS case applied at the beginning of the duct has the least flow distortion. In addition, it was confirmed that when BLS was applied around the cowl lip, the flow distortion was severe and the flow distortion was reduced again after the cowl lip. As the distance from the cowl lip increases, it is confirmed that it converges to the DC60 value of the basic model, which does not have BLS. It can be seen that the effect of BLS occurs before location 0.14. This indicates that the effect of BLS is small after location 0.14.

3.3 Velocity Profile

Figure 8 shows the velocity profile by dividing the section by 0.5 unit from X/D_{EF} 1 to 2.5. The velocity profiles were analyzed by using three cases [base, PS (0,0.1),

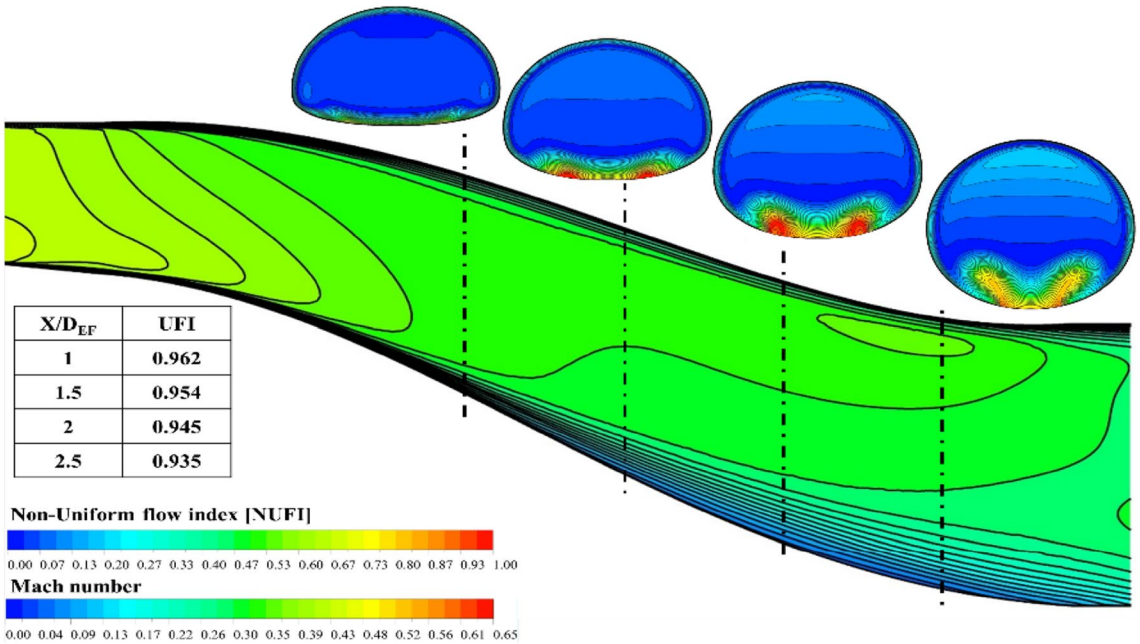

Fig. 6 Aerodynamic characteristics on the S-Duct with inlet shape AR (0.75,0)

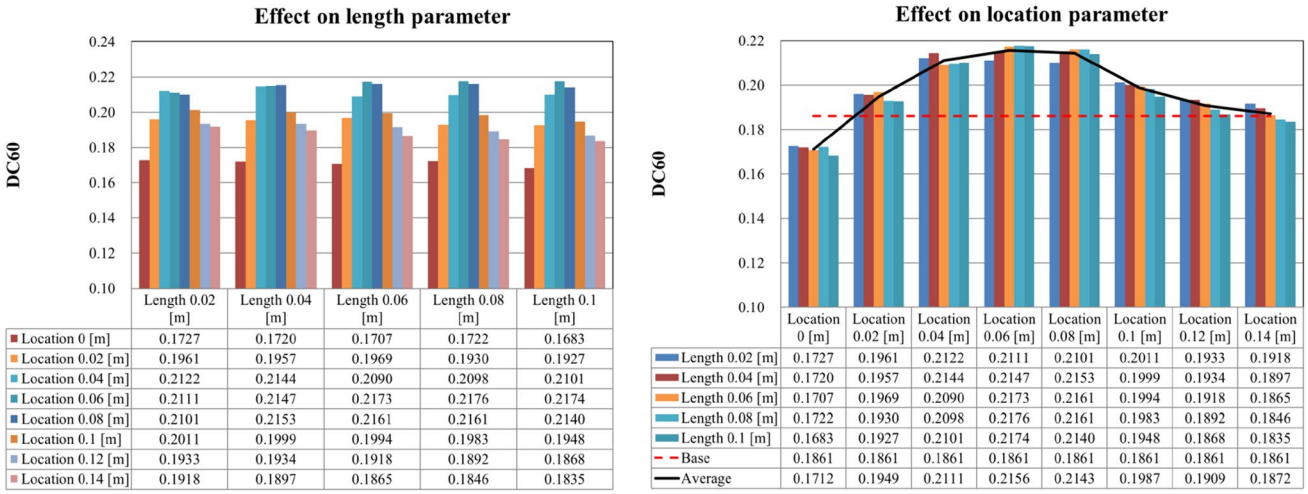

	Length 0.02 [m]	Length 0.04 [m]	Length 0.06 [m]	Length 0.08 [m]	Length 0.1 [m]
Location 0 [m]	0.1727	0.1720	0.1707	0.1722	0.1683
Location 0.02 [m]	0.1961	0.1957	0.1969	0.1930	0.1927
Location 0.04 [m]	0.2122	0.2144	0.2090	0.2098	0.2101
Location 0.06 [m]	0.2111	0.2147	0.2173	0.2176	0.2174
Location 0.08 [m]	0.2101	0.2153	0.2161	0.2161	0.2140
Location 0.1 [m]	0.2011	0.1999	0.1994	0.1983	0.1948
Location 0.12 [m]	0.1933	0.1934	0.1918	0.1892	0.1868
Location 0.14 [m]	0.1918	0.1897	0.1865	0.1846	0.1835

	Location 0 [m]	Location 0.02 [m]	Location 0.04 [m]	Location 0.06 [m]	Location 0.08 [m]	Location 0.1 [m]	Location 0.12 [m]	Location 0.14 [m]
Length 0.02 [m]	0.1727	0.1961	0.2122	0.2111	0.2101	0.2011	0.1933	0.1918
Length 0.04 [m]	0.1720	0.1957	0.2144	0.2147	0.2153	0.1999	0.1934	0.1897
Length 0.06 [m]	0.1707	0.1969	0.2090	0.2173	0.2161	0.1994	0.1918	0.1865
Length 0.08 [m]	0.1722	0.1930	0.2098	0.2176	0.2161	0.1983	0.1892	0.1846
Length 0.1 [m]	0.1683	0.1927	0.2101	0.2174	0.2140	0.1948	0.1868	0.1835
Base	0.1861	0.1861	0.1861	0.1861	0.1861	0.1861	0.1861	0.1861
Average	0.1712	0.1949	0.2111	0.2156	0.2143	0.1987	0.1909	0.1872

Fig. 7 Flow distortion coefficient to the effect of BLS factor

PS (0.06,0.08)] with a large performance difference. PS (0,0.1) and PS (0.08,0.06) are defined as a parameter [position 0 (m), length 0.1 (m)] and parameter [position 0.08 (m), length 0.06 (m)] defined by parameter study (location, length). It can be seen that the velocity of the flow increases as the internal flow of the duct moves closer to the engine face, and the core of the flow is shifted toward the port side from the center. As shown in Fig. 8, the flow has a loss of energy due to the curvature of the duct, so the core of the flow is biased to one side. Also, when comparing the velocity profiles of each section, it was shown that the boundary layer thickness increases as the engine face is close. Compared with the other cases, the thickness of the boundary layer was the thinnest in the PS (0,0.1) case. As performed by Wagner et al. [7, 8], the thickness of the boundary layer affects the quality of flow and a thinner boundary layer yields better performance. The PS (0.06,0.08) case showed the worst performance in this study, as the boundary layer thickness of the PS (0.06,0.08) case from X/D_{EF} 1 to X/D_{EF} 2.5 becomes thicker than the base case where BLS is not applied.

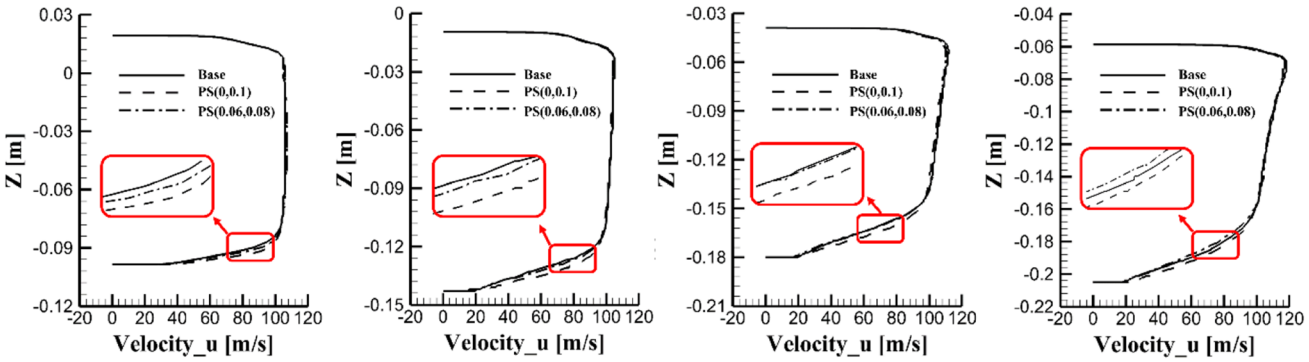

Fig. 8 Velocity profile at each section

3.4 Normalized Total Pressure Contour for Each Section

Figure 9 is a contour comparing the total pressure coefficient of each section ($X/D_{EF}=1.5$, 2, 2.5, engine face) for a base, worst (location 0.06, length 0.08), and best (location 0, length 0.1) case. From $X/D_{EF}=1.5$ to the engine face, it was confirmed that a counter-rotating vortex was developed on the starboard side. It was also confirmed that the low-pressure area about each section gradually converges to the center of starboard side. In the $X/D_{EF}=1.5$ region, the base case showed a total pressure irregularity similar to other cases. However, as the flow approaches the engine face, the PS (0.06,0.08) case showed a large total pressure irregularity. A counter-rotating vortex was generated from $X/D_{EF}=2$. In addition, it was also possible to judge the degree of dispersion of the counter-rotating vortex at $X/D_{EF}=2.5$. The PS (0,0.1) case with the smallest flow distortion has the smallest counter-rotating vortex and was located at the farthest point from the starboard side.

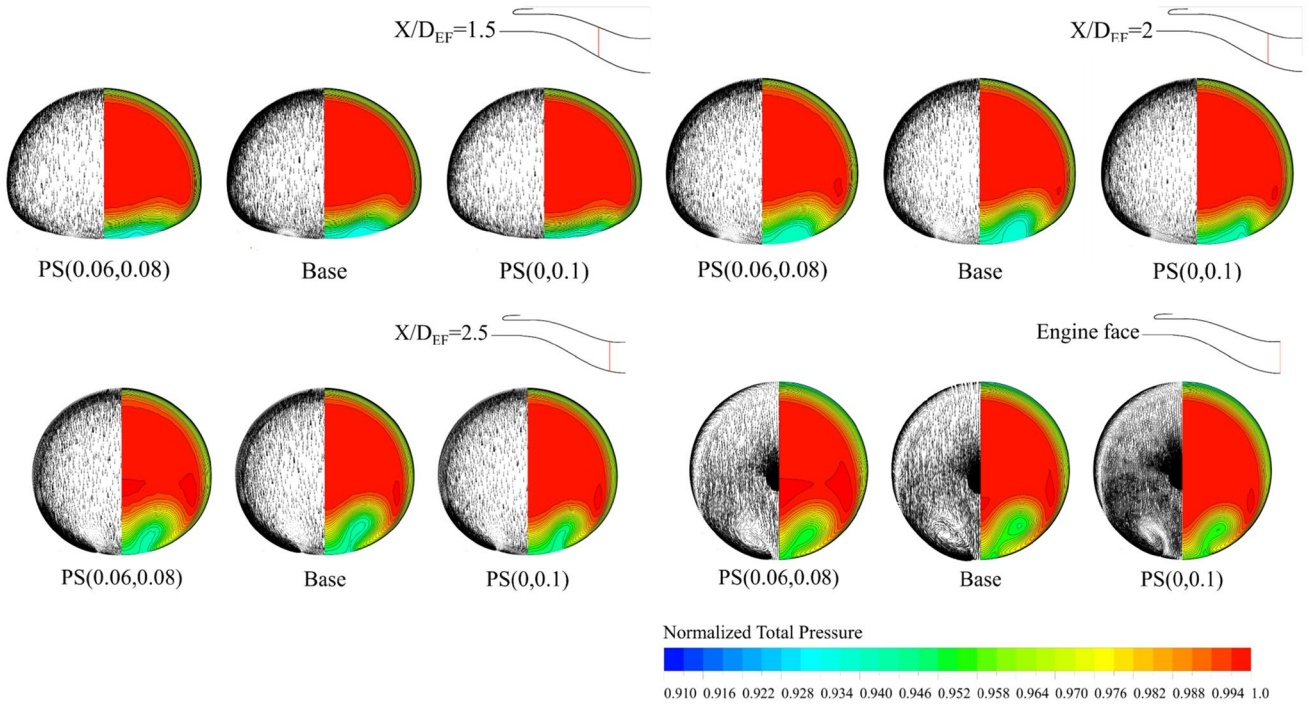

Fig. 9 Normalized total pressure contour for each section

4 Conclusions

In this study, computational analysis has been performed for investigating the effect of the boundary layer suction near the S-duct inlet on the flow distortion of the S-duct and the inflow of the engine.

In order to form a uniform flow field at the engine face, it is important to control the flow distortion caused by the counter-rotating vortex. The strength of the vortex and the flow distortion on the engine face were influenced according to the position and length of the boundary layer suction. The shorter the length of the boundary layer suction face was, the smaller the flow distortion was, but the effect was not great. On the other hand, it was confirmed that the degree of the flow distortion varies greatly according to the position of the boundary layer suction face, and the flow distortion becomes larger as the suction face was near the cowl lip.

In conclusion, this study has confirmed the possibility of improving the flow distortion of the S-duct using the boundary layer suction. Based on this study, we will investigate more detailed flow distortion structure by changing boundary layer suction flow and inflow condition.

References

1. Plas AP (2006) Performance of a boundary layer ingesting propulsion system. MS Thesis. Dept. of Aeronautics and Astronautics, Massachusetts Institute of Technology
2. Saha K, Singh SN, Seshadri V (2007) Computational analysis on flow through transition S-diffusers: Effect of inlet shape. J Aircr 44:187–193
3. Menzies R (2001) Computational investigation of lows in difusing S-shaped intakes. Acta Polytechnica 41(3–4):61–67
4. Menzies R (2002) Investigation of S-shaped intake aerodynamics using computational fluid dynamics. Ph.D. Thesis, Dept. of Aerospace Engineering, University of Glasgow
5. Choi MS, Park JY, Baek JH (2005) Effects of the inlet boundary layer thickness on the flow in an axial compressor (I)—hub corner stall and tip leakage flow. Trans Korean Soc Mech Eng B 29(8):948–955
6. Choi MS, Park JY, Baek JH (2005) Effects of the inlet boundary layer thickness on the flow in an axial compressor (II)—loss mechanism. Trans Korean Soc Mech Eng B 29(8):956–962
7. Wagner JH, Dring RP, Joslyn HD (1983) Axial compressor middle stage secondary flow study. NASA CR-3701
8. Wagner JH, Dring RP, Joslyn HD (1985) Inlet boundary layer effects in an axial compressor rotor: part 1, 2. J Eng Gas Turbines Power 107:374–386
9. Ki DJ (1997) An experimental study on the intake boundary layer diverters for transonic aircraft. J Korean Soc Aeronaut Space Sci 25(6):14–22
10. Debiasi M, Herberg MR, Yan Z, Dhanabalan SS, Tsai HM (2008) Control of flow separation in S-ducts via flow injection and suction. In: 46th AIAA aerospace science meeting and exhibition
11. Scribben AR, Wing NG, Burdisso R (2006) Effectiveness of a serpentine inlet duct flow control technique at design and off-design simulated flight conditions. J Turbomach 128:332–339
12. Choi JH, Cheon SM, Choe YH, Hong WR, Kim CA (2012) Study on concept design of supersonic inlet and flow control of bleeding under operating condition. J Korean Soc Aeronaut Space Sci 40(12):1025–1031
13. Harloff GJ, Smith GE (1996) Supersonic-inlet boundary-layer bleed flow. AIAA J 34(4):778–785
14. Slater JW (2009) Improvements in modeling 90° bleed holes for supersonic inlets. In: AIAA paper 2009-0710, 47th AIAA aerospace sciences meeting and exhibit, Orlando
15. Willis BP, Davis DO, Hingst WR (1995) Flow coefficient behavior for boundary-layer bleed holes and slots. In: AIAA Paper 95-0031, 33rd AIAA aerospace sciences meeting and exhibit, Reno
16. Willis BP, Davis DO (1996) Boundary layer development downstream of a bleed mass flow removal region. In: AIAA Paper 1996-3278, AIAA/ASME/SAE/ASEE joint propulsion conference and exhibit, Lake Buena Vista
17. Liou MF, Benson TJ (2010) Optimization of bleed for supersonic inlet. In: 13th AIAA/ISSMO multidisciplinary analysis optimization conference
18. Lee JH, Cho JS (2018) Effect of aspect ratio of elliptical inlet shape on performance of subsonic diffusing S-duct. J Mech Sci Technol 32(3):1153–1160
19. Tomas MB, Anne LD, Mattias C, Jaap VM, Roald AQ, Phil T (2012) GARTEUR AD/AG-43 application of CFD high offset intake diffusers. GARTEUR Final Report
20. Lee BJ, Kim CA (2007) Automated design methodology of turbulent internal flow using discrete adjoint formulation. Aerosp Sci Technol 11:163–173
21. Sophia L, Doyle DK (2002) Automated design optimization of a three-dimensional S-shaped subsonic diffuser. J Propul Power 18:913–921
22. Weltens H, Bressler H, Terres F, Neumeier H, Rammoser D (1993) Optimization of catalytic converter gas flow distribution by CFD prediction. SAE paper 930780
23. Tsinoglou DN, Koltsakis GC, Missirlis DK, Yakinthos KJ (2004) Transient modelling of flow distribution in automotive catalytic converters. Appl Math Model 28:775–794
24. ANSYS Release 15 (2013) CFX-solver theory guide. ANSYS Inc
25. Menter FR (1994) Two-equation Eddy viscosity turbulence models for engineering applications. AIAA J 32:1598–1605
26. May NE (1997) The prediction of Intake/S-bend diffuser flow using various two-equation turbulence model variants including non-linear Eddy viscosity formulations. ARA. Contractor Report, M316/1, 1997
27. AGARD (1991) Air intakes for high speed vehicles. AGARD ADVISORY 270, Fluid Dynamics Panel Working Group 13